# Influence of Support Friability and Concentration of α-Olefins on Gas-Phase Ethylene Polymerization over Polymer-Supported Metallocene/Methylaluminoxane Catalysts

**Hassan Hammawa, Sieghard E. Wanke**

*Department of Chemical and Materials Engineering, University of Alberta, Edmonton, Alberta T6G 2G6, Canada*

Received 20 May 2005; accepted 8 June 2006
DOI 10.1002/app.25527
Published online in Wiley InterScience (www.interscience.wiley.com).

**ABSTRACT:** The effects of support friability (Φ) and ethylene/comonomer ratios were investigated over supported metallocene/methylaluminoxane catalysts prepared with nine different porous polymeric supports and various comonomer concentrations with a 2-L reactor operated in the semibatch gas-phase mode at 80°C and 1.4 MPa. Φ of the supports was measured with a newly devised method. The performance of the supported catalysts depended on support Φ as follows. The average homopolymerization activities varied from less than 6 t of polyethylene (PE) (mol of Zr)$^{-1}$ h$^{-1}$ for low-Φ catalysts to 10–20 t of PE (mol of Zr)$^{-1}$ h$^{-1}$ for moderate-Φ catalysts and up to 100 t of PE (mol of Zr)$^{-1}$h$^{-1}$ for the high-Φ catalysts. The presence of 1-hexene and propylene comonomers increased the activity of the low-Φ catalysts by up to 20-fold and 50-fold, respectively; that is, there were very marked comonomer effects. Activity enhancement by 1-hexene was less than 3-fold for the moderate-Φ catalysts, whereas the high-Φ catalysts showed little activity enhancement. Sometimes, 1-hexene even resulted in activity reductions. Very different particle morphologies were obtained with the catalysts of different Φ's. © 2007 Wiley Periodicals, Inc. J Appl Polym Sci 104: 514–527, 2007

**Key words:** metallocene catalysts; morphology; polyethylene (PE)

## INTRODUCTION

Soon after the discovery of the effectiveness of the metallocene/methylaluminoxane (MAO) catalyst system in olefin polymerization in the late 1970s, it was realized that the new catalyst system must be supported on solid carriers for maximum benefit to the polyolefin industry. Supporting the homogeneous metallocene/MAO catalysts reduces the MAO requirement and reactor fouling and improves the morphology of the resulting polymer product. In addition, supported catalysts are readily usable in existing industrial slurries and gas-phase reactors.

The immobilization of metallocene/MAO systems on solid carriers is normally accompanied by a decrease in catalytic activity. The activity drop has been attributed to (1) geometric restrictions of monomer access to the active sites[1,2] or the limitation of metallocene–MAO interaction due to isolated confinement;[3] (2) the deactivation of metal centers during the immobilization, which results in low ratios of active-to-total transition metal centers;[4,5] and (3) a decrease in the propagation rate.[6] Occasionally, supported metallocene/MAO catalysts exhibit higher average activities than homogeneous ones due to more stable kinetic profiles.[4]

It has long been known that catalyst morphology has a strong influence on the initial fragmentation and, hence, polymerization behavior of supported catalysts.[7,8] McDaniel[9] observed increases in the polymerization activity with increasing porosity of silica-supported chromium and Ziegler–Natta catalysts. However, regardless of the porosity, the active catalysts fragmented within the first few minutes of polymerization to a final fragment size of 7–10 μm, whereas activity increased for much longer; therefore, he concluded that fragmentation is a requisite for activity, but it is not the rate-controlling step. More recently, Fink's group[10] demonstrated the importance of particle fragmentation in propylene polymerization over a silica-supported metallocene/MAO catalyst. All of the distinct stages of the polymerization rate profile were directly associated with various stages of fragmentation of the catalyst particles.[10]

More extensive work has been done on the effect of α-olefin comonomers on ethylene polymerization activity; α-olefins, such as $C_3H_6$, 1-$C_4H_8$, 1-$C_6H_{12}$, and

*Correspondence to:* H. Hammawa, Department of Chemical and Petroleum Engineering, University of Calgary, Calgary, Alberta T2N 1N4, Canada (hhammawa@ucalgary.ca).

Contract grant sponsor: Natural Sciences and Engineering Research Council of Canada.
Contract grant sponsor: NOVA Chemicals Corp.

1-$C_8H_{16}$, usually enhance the activity of Ziegler–Natta and metallocene/MAO-catalyzed ethylene polymerization.[11,12] The comonomer enhancement has been attributed to physical and chemical effects. The physical effects include the fracturing of the catalyst particle to expose new active sites[13–15] and the enhanced diffusion of monomer molecules through the semicrystalline ethylene/α-olefin copolymer encapsulating the catalyst particles.[16] Chemically, α-olefins are thought to participate in the formation of new catalyst sites and/or the activation of dormant sites[17,18] and in the increase of the propagation rate constant.[19,20]

Ethylene/α-olefin synergism seems to occur only in nonhomogeneous polymerization systems, that is, polymerization over supported catalysts[21] or initially homogeneous systems in which the polymer formed is insoluble in the solvent and precipitates out of the solution.[11,22] When the polymer precipitates from an initially homogeneous system, the active center becomes encapsulated in the precipitated polymer. In truly homogeneous olefin polymerization systems where both the catalyst and the polymer product remain in solution, there is no comonomer enhancement; often, negative comonomer effects are observed.[11,16]

Most investigations on heterogeneous metallocene/MAO catalysts have been based on silica-supported catalysts in slurry polymerization, even though polymeric supports present a better environment for the immobilization of metallocene catalysts, and gas-phase processes have greater economic and environmental advantages over the slurry ones. In none of the above investigations has the catalyst performance been directly related to its friability (Φ). McDaniel[9] qualitatively implied an increase in Φ with the silica porosity; however, the porosity and Φ of polymeric support particles can be independently controlled from the preparation recipe.[23] The objective of this study was, therefore, to quantify Φ of polymeric supports and investigate its influence on the gas-phase polymerization activity and product morphology of the supported catalyst.

## EXPERIMENTAL

### Materials

The supports and catalysts are described in Table I. Four of the supports (Sup-1, Sup-7, Sup-8, and Sup-9) were synthesized in our laboratory; details of the synthesis procedure were presented by Zhou et al.[24] Sup-2 to Sup-5 were HayeSep types S, R, A, and B, respectively, purchased from HayeSep Separations, Inc. (Bandera, TX), and Sup-6 was Porapak type T purchased from Chromatographic Specialties, Ltd. (Brockville, Ontario, Canada). All other reagents and materials were the same as those described previously.[25]

### Catalyst preparation

The catalyst preparation procedure was described previously.[25] Briefly, the desired amount of support was placed in a three-necked flask and heated (at 70–85°C) with evacuation for about 17 h. The evacuated support was cooled to room temperature, suspended in 5–10 mL of anhydrous toluene, and reacted with a predetermined amount of the MAO solution for 2–3 h at room temperature. The metallocene solution prepared by the dissolution of the desired amount of (*n*-$BuCp)_2ZrCl_2$ in 5 mL of anhydrous toluene was added to the support/MAO suspension and allowed to react for 1–2 h on a shaker at room temperature. The final suspension was dried by solvent evacuation to obtain the supported catalyst. Scanning electron

**TABLE I**
**Composition and Properties of the Supports and the Supported Catalysts**

| | Support | | | Catalyst morphology | | | Catalyst composition | | |
|---|---|---|---|---|---|---|---|---|---|
| Catalyst | Name | Composition | Φ (%) | $S_{BET}$ ($m^2/g$) | $V_{Pore}$ ($cm^3/g$) | $R_{Pore}$ (nm) | Al (mmol/g) | Zr (μmol/g) | Al/Zr ratio |
| Cat-1 | Sup-1 | HEMA/DVB | nd | 237 | 0.68 | 6.87 | 4.23 | 15.1 | 280 |
| Cat-2 | Sup-2 | DVB/4-VPy | 19.4 | 258 | 0.38 | 7.15 | 3.75 | 17.8 | 210 |
| Cat-3 | Sup-3 | DVB/N-V-2-P | 18.1 | 279 | 0.38 | 5.18 | 4.23 | 19.8 | 215 |
| Cat-4 | Sup-4 | DVB/EGDM | 27.3 | 145 | 0.37 | 6.16 | 4.23 | 11.2 | 380 |
| Cat-5 | Sup-5 | DVB/PEI | 22.1 | 303 | 0.34 | 4.39 | 3.11 | 20.7 | 150 |
| Cat-6 | Sup-6 | EGDM | 16.0 | 112 | 0.26 | 4.31 | 6.12 | 14.0 | 435 |
| Cat-7 | Sup-7 | HEMA/STY/DVB | 43.8 | 15 | 0.14 | 18.30 | 4.34 | 16.7 | 260 |
| Cat-8 | Sup-8 | DVB | 49.7 | 90 | 0.13 | 2.96 | 6.08 | 22.9 | 265 |
| Cat-9 | Sup-9 | HEMA/DVB | 66.0 | 74 | 0.33 | 6.82 | 2.48 | 6.7 | 370 |
| Cat-10 | Sup-9 | HEMA/DVB | 66.0 | 72 | 0.50 | 7.07 | 4.30 | 20.5 | 210 |

HEMA, 2-hydroxyethylmethacrylate; DVB, divinylbenzene; nd, not determined; 4-VPy, 4-vinylpyridine; EGDM, ethylene glycol dimethacrylate; PEI, poly(ethylene imine); N-V-2-P, *N*-vinyl-2-pyrrolidinone; STY, styrene; SBET, specific surface area based on the Brunauer-Emmett-Teller method; VPore, specific pore volume; RPore, pore radius.

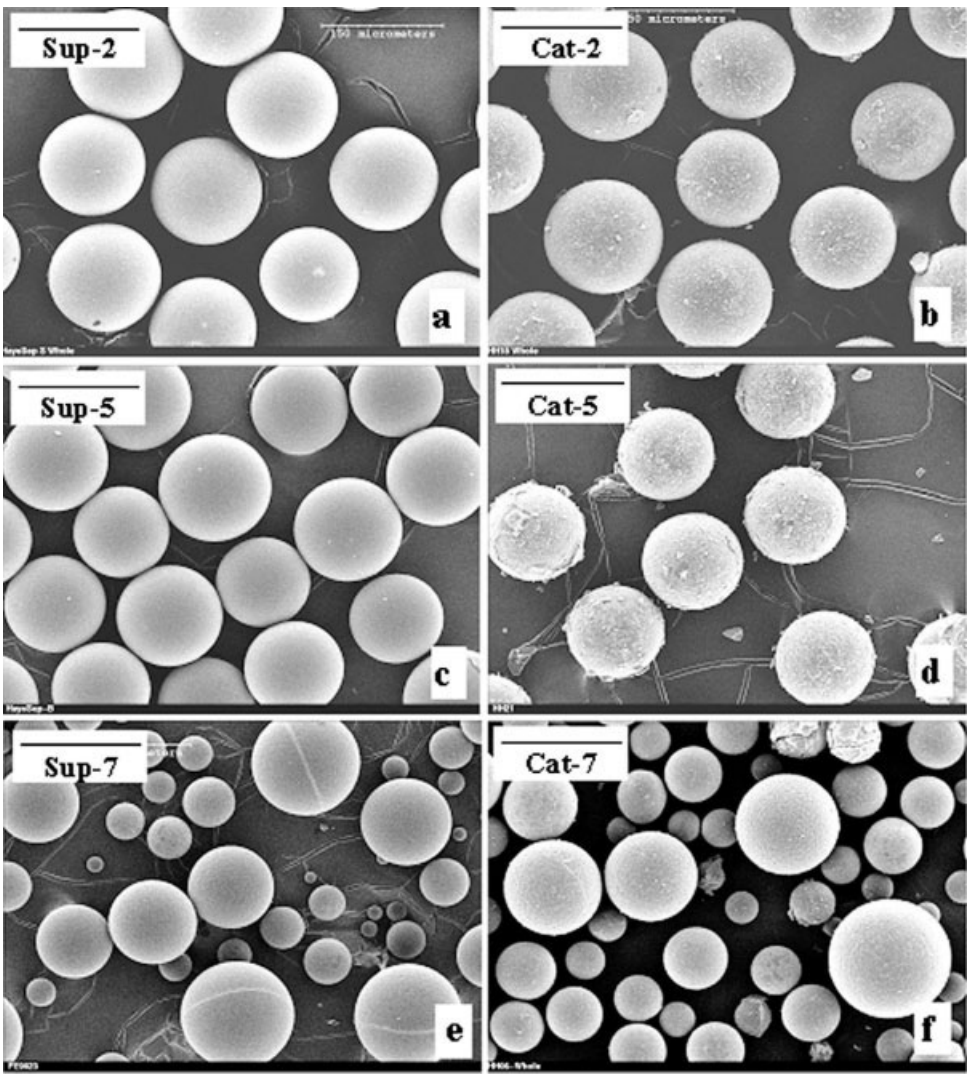


**Figure 1** SEM of representative supports and corresponding supported catalysts. Scale bar: (a)–(d) = 150 μm and (e) and (f) = 300 μm.

micrographs of representative supports and the corresponding supported catalysts are shown in Figure 1.

### Al and Zr analysis

The Al and Zr contents of the catalysts were measured by (delayed γ) instrumental neutron activation analysis at the University of Alberta SLOWPOKE nuclear reactor facility. For Al analysis, the samples and standards were first irradiated in the SLOWPOKE reactor for 60 s under a flux of $10^{11}$ neutrons $cm^{-2}$ $s^{-1}$, allowed to decay for 120 s, and counted (γ) for 60 s. For zirconium analysis, the samples and standards were irradiated at five times higher flux for 1 h, allowed to decay for about 24 h, and counted for 1 h. The detected energy spectra were converted to mass percentages of Al and Zr in the samples with the calibration made from the spectra of a coal fly ash standard (NIST 1633a) for Al and a standard solution (997 μg of Zr/mL, SCP Science lot no. SC3050827) for Zr, respectively. Standard deviations in the reported catalyst compositions were ±3% of the reported values.

### Support Φ measurement

Support Φ was measured by comparison of the particle size distribution (PSD) of the fresh support to the PSD of the same support after ball milling for 1 min according to the following procedure:

1. Twenty-six stainless steel balls (10 × ¼ in. diameter and $16 \times \frac{3}{16}$ in. diameter) with a total mass of 17.8 g were loaded into a 20-mL glass vial.
2. Support (0.12–0.15 g) was added to the vial, and the vial was capped.
3. The capped vial was mounted on a Maxi-Mix III Thermolyne (Dubuque, IA) shaker (with a

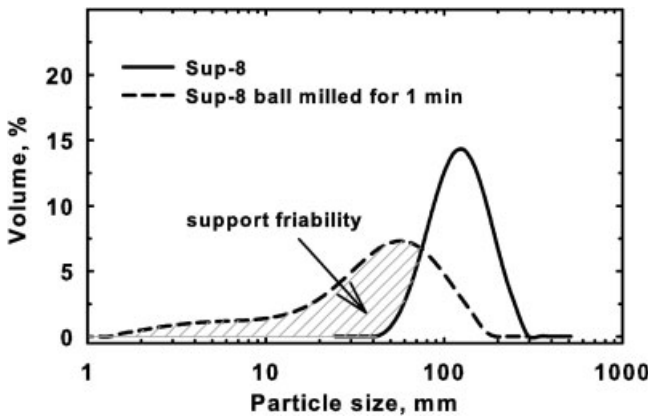


**Figure 2** Φ of Sup-8 from PSDs of fresh and milled samples.

∼ 20-cm Fisher clamp) and milled for 1 min at 800 rpm.
4. Acetone was used to quantitatively recover the pulverized support in a sample bottle.
5. The suspension was dried at room temperature.
6. The dry powder was resuspended in 1–2 mL of ethanol and charged into a Malvern dispersion unit maintained at 3000 rpm (water was the dispersion medium).
7. PSD was acquired (at 10–15% obscuration) twice and averaged.
8. Φ was computed as the volume percentage of pulverized particles lying outside the size range of the original support, as shown by the shaded area of Figure 2.

### Surface areas and pore size distributions

Surface areas and pore size distributions of supports and catalysts were determined by nitrogen sorption measurements at 77 K with an Omnisorp 360 sorptometer (Miami Lakes, FL) operated in the continuous flow mode. The supported catalyst samples were out gassed *in vacuo* for about 1 h at 50°C. This mild outgassing condition was used to keep the catalysts in a state close to the state they entered the polymerization reactor.

### Gas-phase polymerization

Polymerizations were conducted in semibatch mode in a 2-L reactor equipped with gas purification, temperature-control, and data-acquisition systems. A detailed description of the reactor system and the operating procedure were given previously.[25,26] For most polymerization runs, residual tri-isobutyl aluminum (TIBA) scavenger was evacuated from the reactor before the introduction of the catalyst; that is, only trace amounts of TIBA were in the reactor during the polymerization. The total pressure in the reactor was 1.4 MPa for all of the experiments, and the polymerization rate was taken to be the rate of ethylene feed to the reactor required to maintain the pressure at 1.4 MPa.

## RESULTS AND DISCUSSION

The composition and Φ of the polymeric supports are summarized in Table I. Φ of Sup-1 was not measured according to the previous procedure due to limited sample mount. However, qualitative comparison by manual crushing suggested that Φ for Sup-1 was slightly less than that of Sup-2.

All of the supports listed in Table I were nonswellable in toluene, the solvent for catalyst preparation, but the rigid pore network structure of the supports enabled even distribution of the catalyst precursors throughout the catalyst particles. Figure 3 shows an energy-dispersive X-ray (EDX) line scan for aluminum in Cat-2. The zirconium concentration was below the detection limit of the EDX system used, but the zirconium distribution was expected to follow that of aluminum due to the strong chemical interaction between metallocene and MAO, and the smaller size of the former enabled it to diffuse through the support pores even faster than the macromolecular MAO.

The composition of the supports did not appear to have a major influence on the activity of the catalyst. Catalysts with similar support compositions had very different activities (cf. the rates for Cat-1 with those for Cat-9 and Cat-10 in Tables II and III). The support composition of these catalysts was the same, and the Al and Zr contents of Cat-1 were between those of Cat-9 and Cat-10, but the homopolymerization activity of Cat-1 was much lower than the homopolymerization activities of Cat-9 and Cat-10. Hence, the major

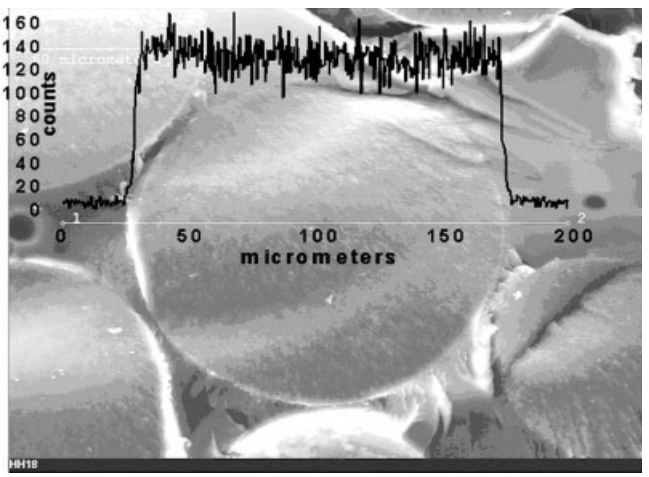


**Figure 3** Aluminum distribution across sectioned Cat-2 particles measured by EDX.

**TABLE II**
**Influence of 1-Hexene on the Polymerization Activity of the Supported Catalysts**

| Run | Catalyst | Amount charged in the reactor | | Initial 1-$C_6H_{12}$ content (mol %) | Activity [t of PE (mol of Zr)$^{-1}$·h$^{-1}$] | | | |
|---|---|---|---|---|---|---|---|---|
| | | 1-Hexane (mol/m$^3$)[a] | Catalyst (mg) | | Average[b] | Maximum[c] | $A_C/A_H$[d] | $t_{Rmax}$ (min)[e] |
| 1 | Cat-1 | 0.0 | 51 | 0.0 | 1.5 | 1.56 | — | 24 |
| 2 | Cat-1 | 13.7 | 50 | 3.0 | 27.6 | 33.8 | 17.3 | 29 |
| 3 | Cat-2 | 0.0 | 77 | 0.0 | 5.6 | 6.6 | — | 5 |
| 4 | Cat-2 | 8.1 | 76 | 1.7 | 26.9 | 30.2 | 4.8 | 31 |
| 5 | Cat-2 | 16.2 | 76 | 3.4 | 48.0 | 61.5 | 8.6 | 28 |
| 6 | Cat-2 | 25.4 | 77 | 5.5 | 20.4 | 21.7 | 3.6 | 40 |
| 7 | Cat-4 | 0.0 | 84 | 0.0 | 20.5 | 25.4 | — | 22 |
| 8 | Cat-4 | 7.4 | 80 | 1.5 | 30.9 | 45.5 | 1.5 | 22 |
| 9 | Cat-4 | 15.2 | 80 | 3.2 | 31.1 | 45.3 | 1.5 | 21 |
| 10 | Cat-5 | 0.0 | 75 | 0.0 | 10.2 | 24.5 | — | 4 |
| 11 | Cat-5 | 8.5 | 78 | 1.8 | 27.9 | 40.0 | 2.7 | 9 |
| 12 | Cat-5 | 15.2 | 85 | 3.3 | 30.0 | 44.4 | 2.9 | 13 |
| 13 | Cat-5 | 22.9 | 78 | 4.9 | 12.8 | 14.4 | 1.3 | 10 |
| 14 | Cat-6 | 0.0 | 107 | 0.0 | 16.6 | 20.8 | — | 15 |
| 15 | Cat-6 | 11.6 | 104 | 2.5 | 48.4 | 74.4 | 2.9 | 17 |
| 16 | Cat-6 | 18.7 | 106 | 4.0 | 19.4 | 19.4 | 1.2 | 34 |
| 17 | Cat-7 | 0.0 | 112 | 0.0 | 12.3 | 55.6 | — | 2 |
| 18 | Cat-7 | 10.6 | 113 | 2.3 | 21.0 | 30.1 | 1.7 | 13 |
| 19 | Cat-7 | 21.1 | 113 | 4.5 | 15.4 | 17.2 | 1.3 | 39 |
| 20 | Cat-8 | 0.0 | 32 | 0.0 | 38.5 | 156.8 | — | 1 |
| 21[f] | Cat-8 | 12.0 | 26 | 2.6 | 110.4 | 190.1 | 2.8 | 42 |
| 22[f] | Cat-8 | 15.2 | 52 | 3.3 | 64.0 | 94.0 | 1.7 | 25 |
| 23 | Cat-9 | 0.0 | 31 | 0.0 | 98.7 | 398.7 | — | 3 |
| 24 | Cat-9 | 12.7 | 103 | 2.7 | 109.9 | 165.2 | 1.1 | 11 |
| 25 | Cat-9 | 15.2 | 41 | 3.2 | 39.7 | 63.7 | 0.4 | 15 |
| 26 | Cat-9 | 0.0 | 41 | 0.0 | 103.9 | 299.4 | — | 4 |

[a] Injected once before the start of polymerization.
[b] Calculated from the product recovered (gravimetric).
[c] Based on the measured ethylene flow rate only.
[d] Ratio of average copolymerization to homopolymerization activities.
[e] Time to attain maximum activity.
[f] The TIBA amount in the reactor was 0.28 mmol; there were trace amounts for all other runs.

differences in rate behavior must have been due to factors other than the support composition and Zr and Al contents. In addition, treatment of the support with MAO before metallocene addition during catalyst preparation limited interactions between the metallocene and the support functional groups.[27] Immobilization of the MAO and metallocene reduced the porosity of the catalysts compared to that of the supports (Fig. 4), and the porosity reduction was generally more severe for the smaller pores. Many of the pore size distributions had a sharp peak at pore radii of about 1.8 nm. These peaks, marked with an asterisk in Figure 4, were probably an artifact due to instability in the nitrogen desorption process.[28–30] The pore size of the mesoporous molecular sieve supports was shown to influence polymerization activity and comonomer incorporation;[31] however, no correlation was observed between the pore size and the catalytic activities, as reported in Tables II and III. Similarly, the homopolymerization or copolymerization activities did not vary systematically with pore volume, Zr content, or Al/Zr ratio. However, definite trends in polymerization activity were observed with variations in catalyst surface area and support Φ.

Homopolymerization activity increased with support Φ. Catalysts (made from supports) with Φ's greater than 40% were, on the average, more active than those with Φ's less than 30% by greater than four times. For copolymerization, the increase in activity for the catalysts with high Φ was only a factor of 2. The homopolymerization activities for catalysts with a surface areas less than 200 m$^2$/g were several fold higher than those with surface areas greater than 200 m$^2$/g. This inverse variation in activity with surface area was unexpected but was probably due to the correlation of surface area with Φ. Low-surface-area catalysts had a higher macropore volume and were usually more friable than high-surface-area catalysts. The high-Φ supports consisted of aggregations of weakly interconnected globules, as illustrated in Figure 5. This type of support is obtained when the monomer and the porogen used in the support preparation

**TABLE III**
**Influence of the Comonomer on the Activity of the Catalysts at 80°C and 1.4 MPa**

| | | Amount charged in the reactor | | | | Activity [t of polymer (mol of Zr)$^{-1}$ h$^{-1}$] | | | |
|---|---|---|---|---|---|---|---|---|---|
| | | Comonomer[a] | | | | | | | |
| Run | Catalyst | Type | mol % | Catalyst (mg) | TIBA (mmol)[b] | Average[c] | Maximum[d] | $A_C/A_H$[e] | $t_{R\max}$ (min)[f] |
| 27 | Cat-3 | — | — | 75.0 | Trace | 0.5 | 1.6 | — | 6 |
| 28 | Cat-3 | 1-$C_6H_{12}$ | 4 | 100.3 | 0.20 | 9.1 | 10.8 | 19.8 | 58 |
| 29 | Cat-3 | $C_3H_6$ | 17 | 101.0 | 0.20 | 23.8 | 31.7 | 51.6 | 71 |
| 30 | Cat-10 | — | — | 69.5 | 0.28 | 27.0 | 44.9 | — | 37 |
| 31 | Cat-10 | $C_3H_6$ | 16 | 63.0 | 0.28 | 85.6 | 87.8 | 3.2 | 10 |
| 32 | Cat-10 | 1-$C_6H_{12}$ | 3.2 | 59.7 | 0.20 | 58.3 | 92.5 | 2.2 | 21 |

[a] Injected once before the start of polymerization.
[b] Trace denotes that residual TIBA was evacuated after reactor scavenging.
[c] Calculated from the product recovered (gravimetric).
[d] Based on the measured ethylene flow rate only.
[e] Ratio of average copolymerization to homopolymerization activities.
[f] Time to attain maximum activity.

have a high degree of compatibility.[23] Hence, it was Φ that appeared to be mainly responsible for the difference in polymerization activity for the various catalysts.

### Homopolymerization and copolymerization rate profiles

The gas-phase polymerization conditions and average activities for the catalysts listed in Table I are summarized in Tables II and III. The polymerization rate profiles mostly consisted of an initial activity increase to a maximum followed by an activity decline; activity profiles of this type, common to metallocene/MAO catalysts, are illustrated in Figure 6. The initial spikes in the activity profiles were due to reactor fillup with ethylene at the start of polymerization. The presence of 1-hexene mostly resulted in the increases in the average activity, maximum activity, and acceleration (activity growth) period ($t_{R\max}$). The observed influences of 1-hexene on the activity profiles of the supported catalyst are discussed next.

### Compositional drift during copolymerization

All of the 1-hexene for all of the copolymerization runs listed in Tables II and III was added at the beginning of each run; hence, the concentration of 1-hexene in the gas phase decreased with increasing polymerization due to the incorporation of 1-hexene into the polymer and to the absorption of 1-hexene by the produced polymer. The changes in 1-hexene concentration with time affected the activity profiles and polymer composition. To investigate the effect of the compositional drift of 1-hexene, runs in which the gas-phase concentration of 1-hexene was kept relatively constant by the constant addition of 1-hexene throughout the run were carried out. The gas-phase concentration was measured by online gas chromatography; the analysis procedure was described previously.[26] In Figure 7, the activity profile and gas-phase 1-hexene concentration for two such runs, runs 36 and 37, are compared to the results for a similar run, run 38, in which all of the 1-hexene was added at the beginning of the run. The lower panel in Figure 7 shows the variation in the 1-hexene concentration throughout the runs.

The initial gas-phase 1-hexene concentrations were about equal for all of the runs, and for runs 36 and 37, the 1-hexene concentration remained fairly constant throughout the runs. However, for run 38, the gas-phase 1-hexene concentration decreased to about 20% of its initial concentration by the end of the run. This large decrease in 1-hexene concentration was not all due to the consumption of 1-hexene by the reaction because a significant amount of 1-hexene dissolved in the polyethylene (PE) and the amount dissolved increased with reaction time because the amount of polymer in the reactor increased with reaction time. On the basis of temperature-rising elution fractionation analysis, the fraction of the amount of 1-hexene reacted in these runs varied from 45 to 58%.

The large difference in the 1-hexene concentration profiles between the runs with and without changes in 1-hexene concentration did not result in large differences in the shapes of the activity profiles. The increase in the activity during the first 10 min of the runs was due to fracturing of the catalyst particles, which resulted in increased accessibility to catalytic sites. The 1-hexene concentration was relatively constant for this period even if all the 1-hexene was added initially; hence, the activation part of the activity profile was not significantly affected by the comonomer drift. The shape of the deactivation part of the

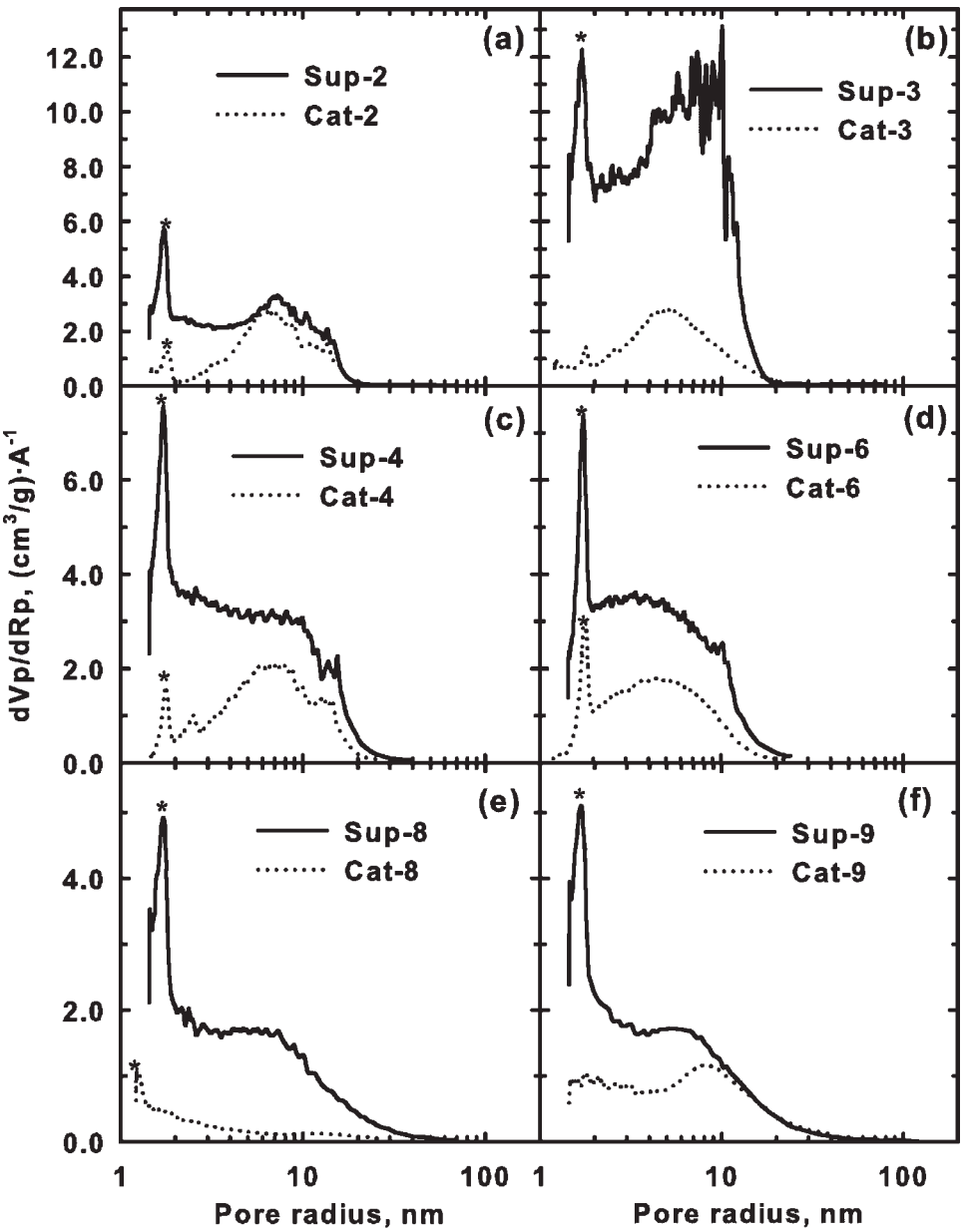


**Figure 4** Pore size distribution of supports and supported catalysts (an asterisk indicates possible artifact peaks). dVp/dRp is the pore size distribution function.

activity profile was relatively insensitive to the mode of 1-hexene addition; that is, the changing 1-hexene concentration was not the main cause of the decrease in polymerization rate after the initial increase in activity. The decrease in the activity was probably due to the loss of active sites. Even though the mode of 1-hexene addition did not significantly affect the activity profiles, it did affect the product composition; that is, the short-chain branching concentration, determined by temperature-rising elution fractionation, for continuous 1-hexene addition (run 37) was 14.3 branches per 1000 carbons, whereas the short-chain branching concentration for the initial batch addition of 1-hexene (run 38) was 6.4.

### Rate profiles of the low-Φ catalysts

Low-Φ (Φ < 30%) catalysts exhibited two distinct polymerization rate behaviors:

1. Low ethylene homopolymerization activities [$A_H$'s; 0.5–5.6 t of PE (mol of Zr)$^{-1}$ h$^{-1}$] and significantly higher ethylene/1-hexene copolymerization activities ($A_C$'s) with $A_C/A_H$ ratios up to 20. Cat-1, Cat-2, and Cat-3, all with Φ < 20%, exhibited this rate behavior (see Tables II and III and Fig. 6).
2. Moderate $A_H$ values [10–20 t of PE (mol of Zr)$^{-1}$·h$^{-1}$] and only moderate activity increases in ethylene/1-hexene copolymerization (Fig. 8).

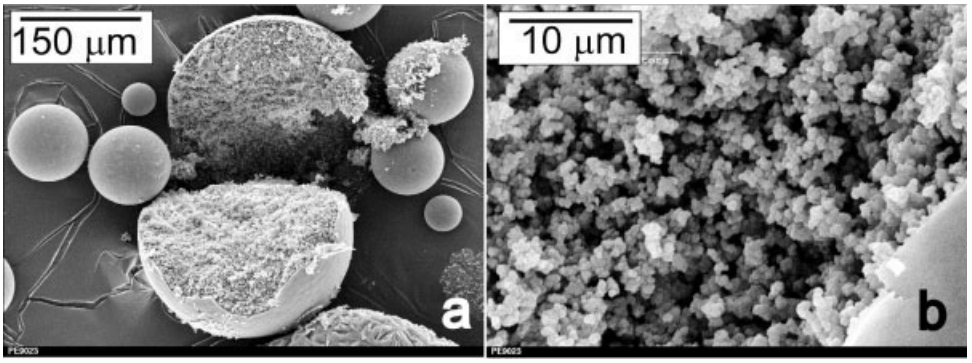


**Figure 5** Internal morphology of the high-Φ support Sup-8 magnified to show the aggregation of globules.

$A_C/A_H$ for these catalysts were all less than 3; Cat-4 and Cat-5, with 20% $\leq \Phi \leq$ 30%, belonged to this group. However, Cat-6, with $\Phi$ = 16%, exhibited similar behavior to the former two probably due to the high Al/Zr ratio of Cat-6.

The activity enhancement during ethylene/1-hexene copolymerization depended on the amount of 1-hexene in the reactor. From Figure 6, the optimum for Cat-2 at 80°C and 1.4 MPa total pressure was about 14 mol/m$^3$ 1-hexene. At higher 1-hexene concentrations, the polymerization activity started to decrease, probably due to high 1-hexene concentration at the active site. A lower reactivity of 1-hexene relative to ethylene would lead to the accumulation of 1-hexene at the active site by the enrichment effect. At high polymerization rates, the bulk gas was convected into the polymerizing particles, where ethylene reacted faster than 1-hexene; this resulted in 1-hexene enrichment in the particle similar to polymerization in the presence of an inert component.[32] The lower activity at high 1-hexene concentrations could also have been due to the softening of the high 1-hexene content copolymer at the prevailing polymerization temperature; this would have rendered it less effective in fracturing the catalyst particle.[31,33–35]

The synergistic effect of α-olefins during ethylene polymerization is widely observed with conventional Ziegler–Natta and metallocene catalysts,[16,36,37] and both physical and chemical effects have been used to explain the phenomenon. Wester and Ystenes[15] observed a significant increase in ethylene polymerization activity over coarsely grained catalyst on propylene addition, but no activity enhancement was observed with the finely grained catalyst, which suggests that physical changes in the catalyst were (at least partly) responsible for the activity enhancement. Our results show that the activity enhancement by 1-hexene and propylene (the comonomer effect) was due to Φ of the support, that is, a physical effect. The presence of the comonomer enhanced the fracturing of catalysts with low Φ's; this is discussed in more detail in the section on product morphology.

### Rate profiles of the high-Φ catalysts

The high-Φ catalysts had high $A_H$ values [up to 100 t of PE (mol of Zr)$^{-1}$ h$^{-1}$], and the maximum activities

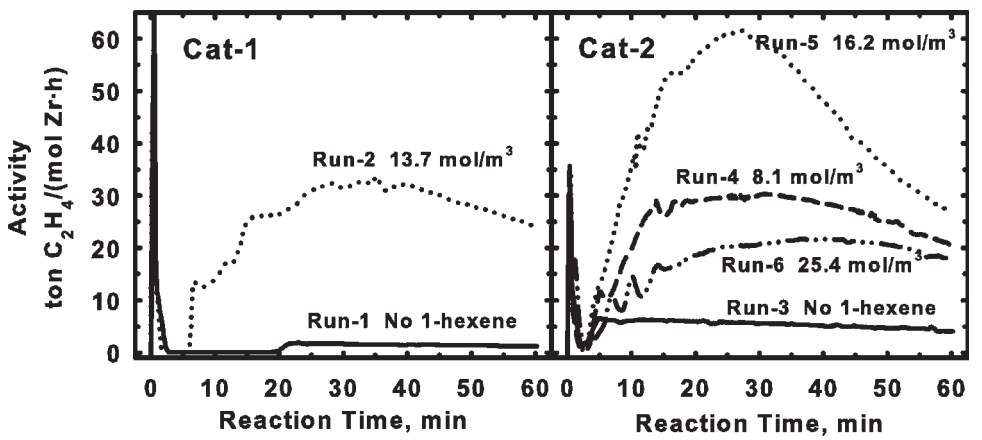


**Figure 6** Effect of the 1-hexene concentration on the gas-phase polymerization activity of low-Φ Cat-1 and Cat-2 at 80°C and 1.4 MPa.

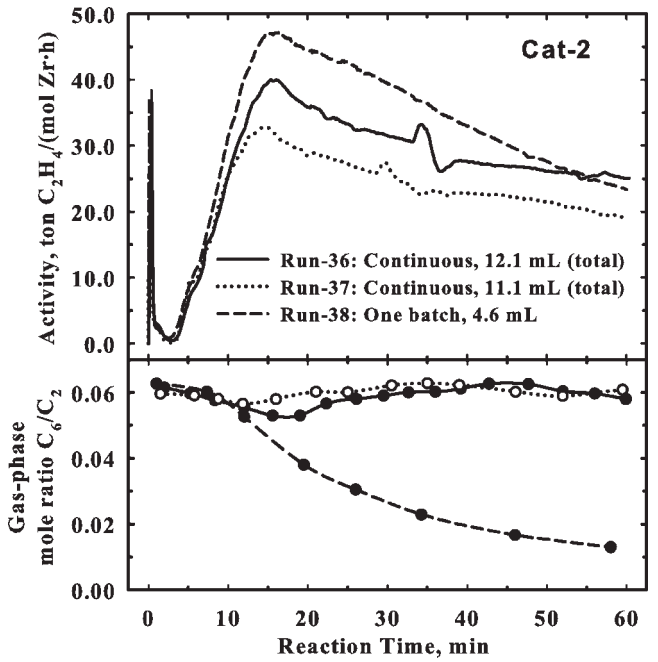


**Figure 7** Polymerization rate profiles and drift in the gas-phase 1-hexene concentration during ethylene/1-hexene copolymerization with batch and continuous comonomer addition (Cat-2 at 80°C and 1.4 MPa).

were attained rapidly ($t_{R\max}$ = 1–4 min). The rapid activity growth indicated that the catalysts fragmented almost instantaneously at the beginning of polymerization. The high-Φ catalysts showed insignificant activity enhancement or even a decrease in activity in the presence of 1-hexene (Fig. 9); the $A_C/A_H$ ratios varied from 0.4 to 2.8. The initial increase in polymerization activity was suppressed by the 1-hexene, but higher average copolymerization activities often occurred due to a broadening of the activity profiles.[38] Maximum copolymerization activities were often lower than the maximum homopolymerization activities. The higher polymerization rates normally obtained with the high-Φ catalysts often resulted in inadequate reactor temperature control. As shown Figure 9, run 21 exhibited the highest temperature excursion; the average, maximum, and minimum gas-phase temperatures measured at 3–10 s intervals for run 21 were 83.0, 101.6, and 78.3°C, respectively. The corresponding values for run 25 were 80.0, 82.6, and 79.8°C, respectively. For all of the other runs with low-Φ catalysts, the temperature increases never exceeded 1°C. Substantial increases in the reactor temperature affected the activity profile; however, this did not change the observed trend in the polymerization rates and, hence, the conclusions drawn from these results.

### Morphology of the homopolymer and copolymer particles

The scanning electron microscopy (SEM) images shown in Figure 10 revealed a completely different morphology of the homopolymer than the copolymer particles from the low-Φ catalysts. Cat-1 (low homopolymerization activity) produced homopolymer particles with embedded cores quite distinct from the surrounding artichoke-like macroporous PE layer [Fig. 10(b)]. EDX line scans (see Fig. 11) clearly showed high aluminum content in the cores but not in the surrounding PE. Evidently, the cores predominantly consisted of the original catalyst particles and contained very little PE. The low zirconium content of the catalyst particles prevented its analysis by EDX.

Contrary to the homopolymer particles, the internal morphology of the ethylene/1-hexene copolymer particles of Cat-1 [Fig. 10(d)] showed several concentric polymer layers without distinct cores. No aluminum was detected in the copolymer particles by EDX; thus, the original catalyst particles were completely fractured, and the accumulated copolymer diluted the catalyst precursors to undetectable Al concentrations.

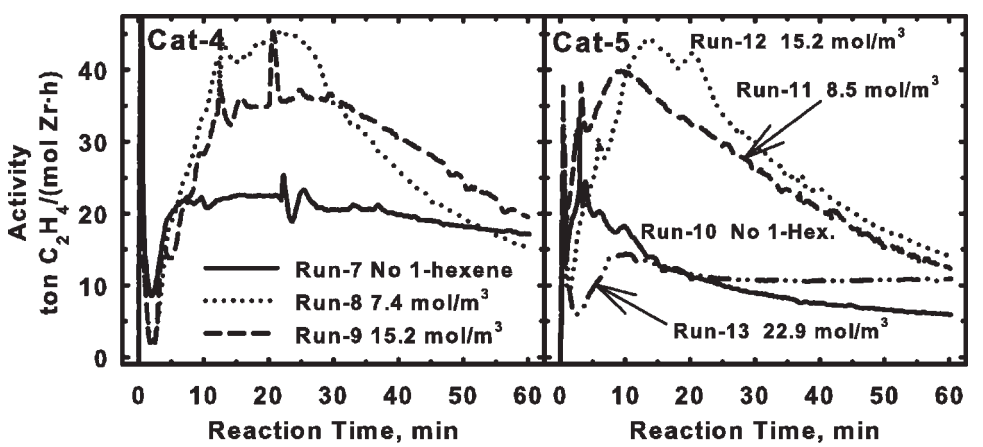


**Figure 8** Effect of the 1-hexene concentration on the gas-phase polymerization activity of moderate-Φ Cat-4 and Cat-5 at 80°C and 1.4 MPa.

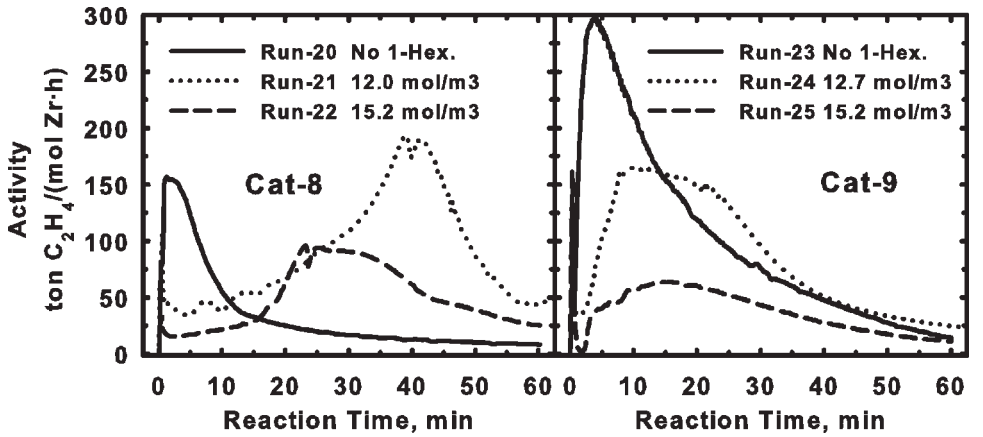


**Figure 9** Effect of the 1-hexene concentration on the gas-phase polymerization activity of high-Φ Cat-8 and Cat-9 at 80°C and 1.4 MPa.

The concentric shell morphology entirely evolved during the copolymerization because the internal morphology of all of the catalysts was uniform.

The homopolymer particles produced by Cat-5 consisted mostly of hollow shells housing a core (Fig. 12). The cores were only weakly attached to the shells and were mostly separated from the hollow shells during particle sectioning for SEM. Cross-sections of the inner cores showed a surrounding polymer layer possibly formed on the initiation of fragmentation from the surface of the catalyst particle. This morphology differed from the artichoke-like morphology of the homopolymer particles shown in Figures 10(b) and 11. The moderate ethylene homopolymerization catalysts rarely produced homopolymer particles with the artichoke-like morphology. The ethylene/1-hexene copolymer particles of these catalysts also showed the concentric shell morphology [Fig. 12(d)].

Figure 13 shows the morphology of polymer particles produced with Cat-9, a high-Φ catalyst. The spherical shape of the catalyst particles was replicated in the polymer particles, and the internal morphology was uniformly porous [Fig. 13(b)]. This morphology was quite consistent with catalysts that fragment rap-

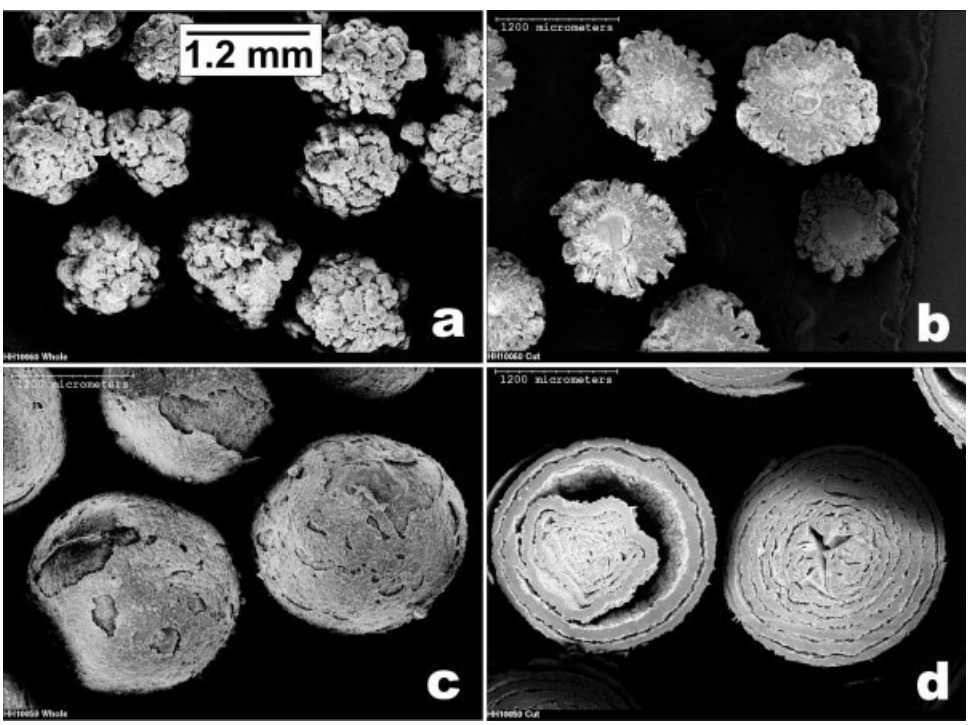


**Figure 10** SEM micrographs of whole (left) and cross-sections (right) of polymer particles produced by Cat-1: (a) and (b) run 1with no 1-hexene and (c) and (d) run 2 with 13.4 mol/$m^3$ 1-hexene.

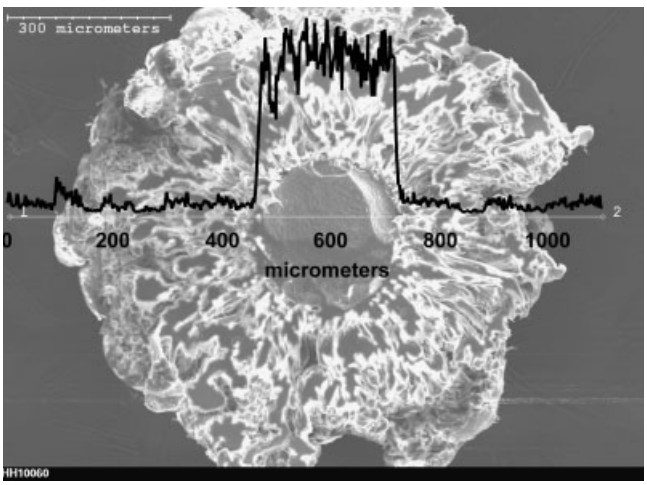


**Figure 11** EDX line scan for aluminum across sectioned PE particle from run 1 revealing unfragmented catalyst cores (Cat-1, 1 h of polymerization, yield ≈ 22 g of PE/g cat).

idly into uniformly sized subparticles that grow at the same rate.[39] The high polymerization rates associated with this rapid catalyst fragmentation at the beginning of polymerization resulted in high ethylene flow rates that eliminated the initial reactor fillup spikes normally observed on the rate profiles (cf. run 20 in Fig. 9 to runs 1–6 in Fig. 6). The internal morphology of most ethylene/1-hexene copolymer particles produced with 15 mol/m$^3$ 1-hexene in the reactor was also uniformly porous, similar to the ethylene homopolymer morphology. The high-Φ catalysts showed an increasing tendency to produce copolymer particles with the concentric shell morphology when the amount of 1-hexene in the reactor exceeded 15 mol/m$^3$, but below this concentration, a uniform internal morphology predominated. Comparatively, the low-Φ Cat-2 produced copolymer particles with the concentric shell morphology with only 8 mol/m$^3$ 1-hexene in the reactor. Thus, the high-Φ catalysts had less of a tendency to produce the layered copolymer particle morphology than the low-Φ catalysts.

The observed morphology variations strongly suggest that the support/catalyst properties influenced the polymerization activity of the polymer-supported catalysts, and the presence of 1-hexene modified the activity and morphology of the resulting polymer particles. The morphology of polymer particles shown in Figures 10–13 did not vary with polymerization temperature or monomer pressure,[38] which signified that it was an inherent property of the catalysts. The sizes of the unfragmented catalyst cores in the homopolymer particles were within the size range of the catalyst particles; hence, little or no fracturing of the catalyst particles occurred.

### Proposed catalyst fracture mechanism during ethylene homopolymerization

The morphologies of homopolymer particles produced over the low-Φ catalysts suggested that when the catalyst particles were exposed to ethylene in the reactor, polymer started to form throughout the cata-

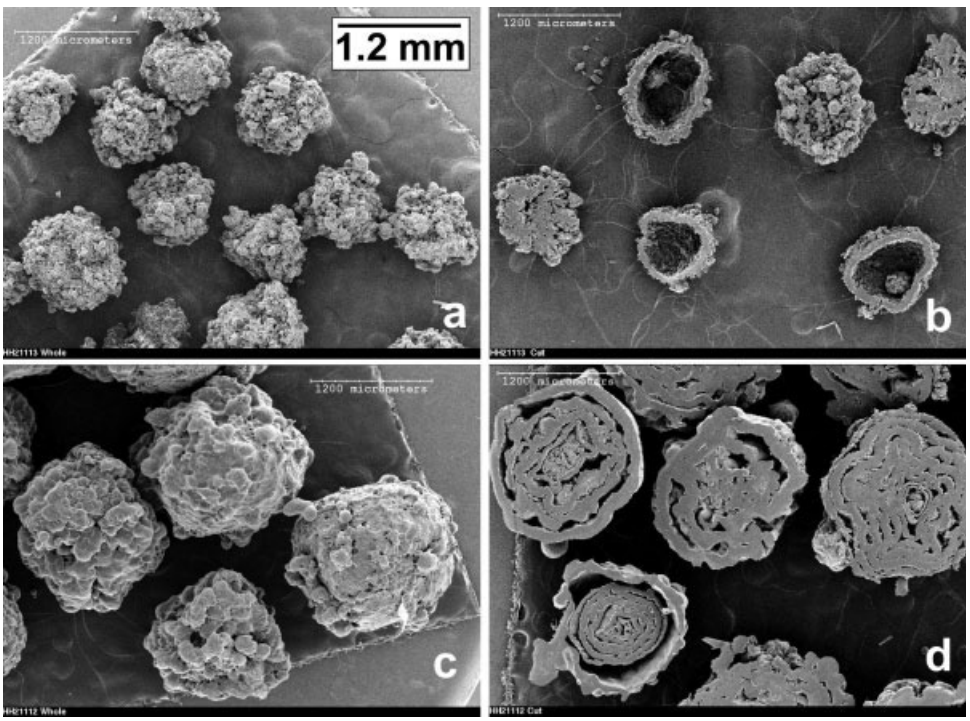


**Figure 12** SEM micrographs of the external surface (left) and cross-section (right) of polymer particles produced by Cat-5: (a) and (b) run 10 with no 1-hexene and (c) and (d) run 12 with 15.2 mol/m$^3$ 1-hexene.

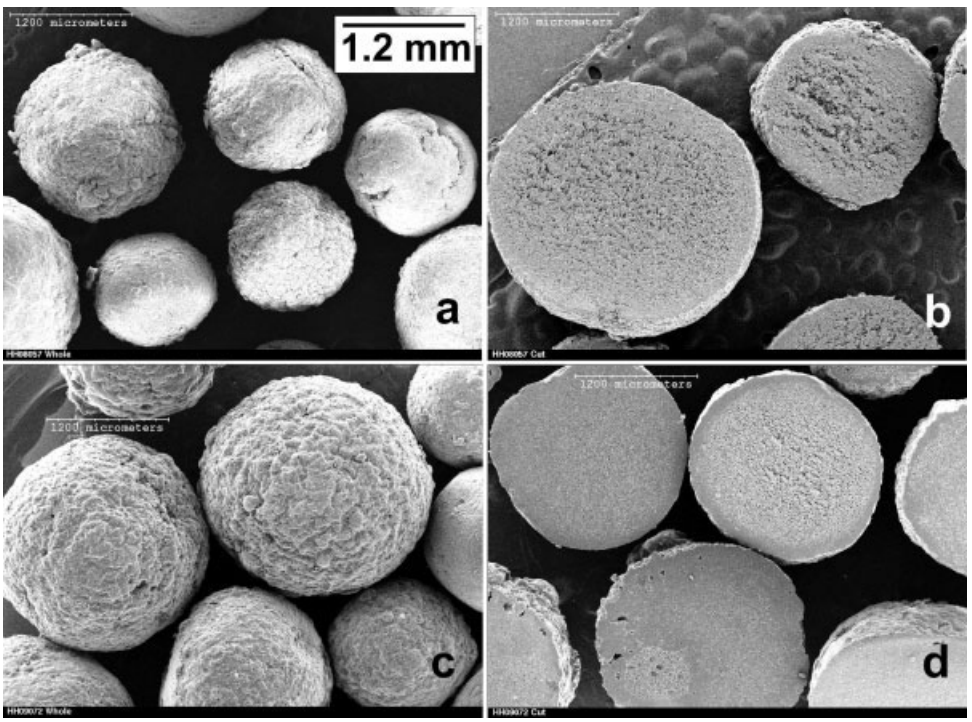


**Figure 13** SEM micrographs of the external surface (left) and cross-section (right) of polymer particles produced by Cat-9: (a) and (b) run 20 with no 1-hexene and (c) and (d) run 22 with 15.2 mol/$m^3$ 1-hexene.

lyst particles, and the outer layer of the catalyst particles fragmented. The accumulating polymer filled up the macropores in the unfragmented catalyst with high-density, crystalline PE, and the strength of the catalyst matrix prevented further fracturing of the catalyst particles [Fig. 14(a)]. This severely limited ethylene diffusion into the catalyst macroparticles; hence, polymerization activity remained low. Poor breakup catalysts were reported to develop strong mass transfer resistance at the microparticle level.[40] The polymerization rates of such catalysts are very low for want of monomer at the active sites.[41,42] The artichoke structure of the polymer around the catalyst core was probably produced by polymerization on the external surface of the catalyst particle in combination with small fragments of catalyst breaking off the external

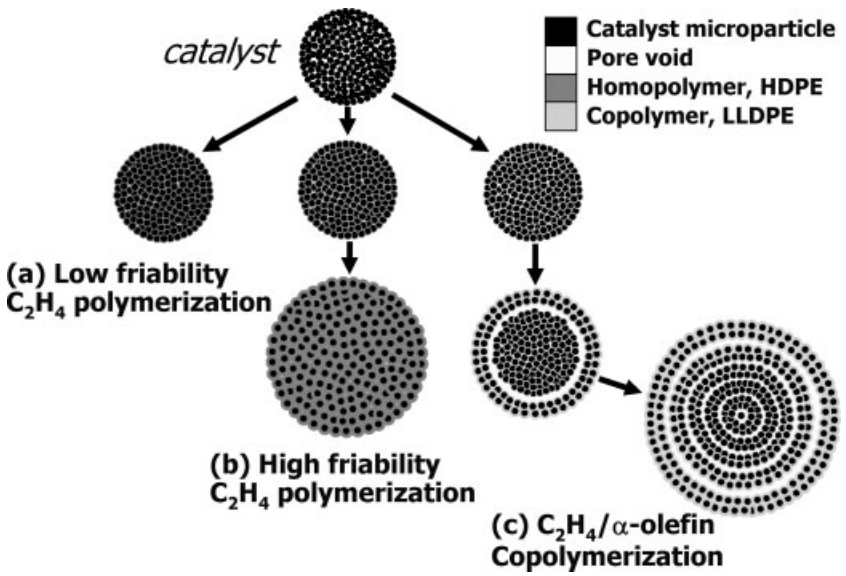


**Figure 14** Proposed fracture mechanism of low- and high-Φ polymer-supported metallocene/MAO catalyst particles during gas-phase olefin polymerization. (HDPE, high density polyethylene; LLDPE, linear low density polyethylene).

surface of the catalyst without fracturing inside the catalyst particles.

The surface area of Cat-1 (237 $m^2/g$) decreased to a negligible value after polymerization to a yield of 22 g of polymer/g of catalyst, probably due to the filling of the pores with PE. In addition, the catalyst cores were easily hand-sectioned with a scalpel, an action that would normally crumble the brittle catalysts particles; thus, the polymer formed in the catalyst pores held the catalyst subparticles together. McDaniel[9] and Dalla Lana et al.[43] observed very low ethylene polymerization activities over silica-supported Phillips catalysts due to mass-transfer limitations. Webb et al.[41] noted that a polymer yield of 0.1 g/g of catalyst rendered the active sites on a silica-supported chromium oxide catalyst inaccessible to ethylene. The fragmentation of the outer layer of the catalyst particles was similar to the initiation of shellwise fragmentation of the catalyst particle from surface to the center as proposed by Bonini et al.[44]

Once the ethylene transport hindrance by the high-crystallinity polymer in the pores of the catalyst cores occurred, manipulation of the polymerization conditions was ineffective in improving activity. Ethylene homopolymerization at 2.8 MPa with Cat-2 showed no activity improvement over the run at 1.4 MPa. In addition, delaying 1-hexene injection until 15 min after the commencement of ethylene homopolymerization did not improve the polymerization activity compared with runs without any added 1-hexene.

When the high-Φ catalysts were exposed to ethylene in the reactor, polymerization and catalyst fragmentation commenced throughout the catalyst particle, as in the widely used multigrain model (Hutchinson et al.[45]). The high Φ of these catalysts enabled the fragmentation process to keep pace with the polymerization rate; hence, the polymer grew evenly in the polymerizing particle, and the particle macroporosity was maintained [Fig. 14(b)]. At high polymerization rates, ethylene transport into the particle occurred by both convection and diffusion. It was previously shown that the presence of nitrogen reduced the polymerization activity relative to a pure ethylene run (both at same ethylene pressure) due to the enrichment effect.[25]

### Fracture mechanism during ethylene/α-olefin copolymerization

During ethylene/α-olefin polymerization, the fracturing of catalyst particles started in a similar manner as the fracturing in homopolymerization, but the catalyst pores were filled up with linear low-density polyethylene (LLDPE). The moderate monomer diffusion rate in the LLDPE created a monomer concentration gradient that resulted in a differential expansion rate of the polymerizing particles. The differential growth rate generated tension in the outer layer of the unfragmented core. When this tension exceeded the yield limit of the catalyst/polymer matrix, the outer layer fragments and the new core surface were exposed to the bulk monomer concentration. Repetition of this layer-by-layer fragmentation of the catalyst particles [Fig. 14(c)] resulted in the concentric shell morphology of the copolymer particles. The tendency of the catalyst particles to form the concentric shell structure decreased with increasing catalyst Φ. Complete fragmentation of the catalyst particles into thin concentric shells occurred early in the polymerization, typically within the first 10 min; subsequently, the fragmented shells grew thicker due to polymer accumulation. Comparatively, Fink et al.[10] reported that over 60 min of polymerization was required for the complete disappearance of the catalyst core during the slurry polymerization of propylene over a silica-supported metallocene catalyst.

According to the previous fracturing models, catalyst Φ and monomer diffusivity were the major factors that determined the polymerization activity and product morphology. The effect of these factors on polymerization activity was further demonstrated by the comparison of ethylene/propylene and ethylene/1-hexene copolymerization with Cat-3 (low Φ) and Cat-10 (high Φ), as summarized in Table III. Residual TIBA was not removed from the reactor after impurity scavenging with 0.2–0.3 mmol of TIBA for all of the runs in Table III, except for run 27. Residual TIBA increased average activity by broadening polymerization rate profiles.[25] However, due to low $A_H$ of low-Φ catalysts, the average activity of run 27 did not change significantly in the presence or absence of residual TIBA. Compared to ethylene homopolymerization, the activity of the low-Φ Cat-3 increased 20-fold in ethylene/1-hexene (~ 4 mol %) and 50-fold in the ethylene/propylene copolymerization with 17 mol % propylene initially present in the reactor. The significantly greater influence of propylene (compared to 1-hexene) on the average activities shown in Table III was due to the higher diffusivity and reactivity of propylene rather than its higher initial concentration in the reactor. For several catalysts tested, decreases in activity with increasing amounts of 1-hexene in the reactor occurred at much lower concentrations than the 17 mol % observed with propylene.[38]

## CONCLUSIONS

Gas-phase $A_H$ of polymer-supported $(n\text{-Bu})_2ZrCl_2$/MAO catalysts increased with support Φ. Lack of fracturing of the low-Φ catalysts during ethylene homopolymerization resulted in a strong mass-transfer limitation and low activity; the presence of 1-hexene or propylene significantly increased the activity. The

magnitude of activity enhancement decreased with increasing catalyst Φ. High-Φ catalysts, which also had high $A_H$, showed little or no activity enhancement by 1-hexene. The activity enhancement by 1-hexene reached a maximum that was catalyst specific. Polymerization activity enhancement by the comonomer decreased with increasing comonomer size due to the diffusivity and the reactivity of the comonomers. The comonomer enhancement for the polymer-supported ($n$-BuCp)$_2$ZrCl$_2$/MAO catalysts was caused by differences in the ease with which the catalyst particles fractured (Φ); that is, the comonomer effect was mainly due to physical effects and not due to chemical effects.

Rapid catalyst fragmentation of high-Φ catalysts ensured adequate porosity in the polymerizing particles; hence, high $A_H$ and uniform particles morphology resulted. During ethylene/α-olefin polymerization, the differential expansion rate of the polymerizing particles led to a layer-by-layer fragmentation that resulted in an onion-ring-like morphology of the polymer particles. The tendency of the catalyst particles to form the onion-ring-like structure decreased with increasing catalyst Φ. The results of this study provide an additional experimental perspective to ongoing modeling efforts in particle fragmentation during olefin polymerization over heterogeneous catalysts.[34,35,46]

## References


1. van Looveren, L. K.; Geysen, D. F.; Vercruysse, K. A.; Wouters, B. H.; Grobet, P. J.; Jacobs, P. A. Angew Chem Int Ed 1998, 37, 517.
2. Michelotti, M.; Altomare, A.; Ciardelli, F.; Roland, E. J Mol Catal A 1998, 129, 241.
3. Woo, S. I.; Ko, Y. S.; Han, T. K. Macromol Rapid Commun 1995, 16, 489.
4. Braca, G.; Sbrana, G.; Raspolli-Galletti, A. M.; Altomare, A.; Arribas, G.; Michelotti, M.; Ciardelli, F. J Mol Catal A 1996, 107, 113.
5. Chien, J. C. W. Top Catal 1999, 7, 23.
6. Harrison, D.; Coulter, I. A.; Wang, S.; Nistala, S.; Kuntz, B. A.; Pigeon, M.; Tian, J.; Collins, S. J Mol Catal A 1998, 128, 65.
7. Whittaker, H. L.; Wills, G. B. J Appl Polym Sci 1969, 13, 1921.
8. Ivanchev, S. S.; Baulin, A. A.; Rodionov, A. G. J Polym Sci Polym Chem Ed 1980, 18, 2045.
9. McDaniel, M. P. J Polym Sci Polym Chem Ed 1981, 19, 1967.
10. Fink, G.; Tesche, B.; Korber, F.; Knoke, S. Macromol Symp 2001, 173, 77.
11. Chien, J. C. W.; Nozaki, T. J Polym Sci Part A: Polym Chem 1993, 31, 227.
12. Camurati, I.; Cavicchi, B.; Dall'Occo, T.; Piemontesi, F. Macromol Chem Phys 2001, 202, 701.
13. Tait, P. J. T.; Downs, G. W.; Akinbami, A. A. In Transition Metal Catalyzed Polymerizations—Ziegler–Natta and Metathesis Polymerizations; Quirk, R. P., Ed.; Cambridge University Press: Cambridge, England, 1988; Chapter 55.
14. Muñoz-Escalona, A.; García, H.; Albornoz, A. J Appl Polym Sci 1987, 34, 977.
15. Wester, T. S.; Ystenes, M. Macromol Chem Phy 1997, 198, 1623.
16. Koivumäki, J.; Seppälä, J. V. Macromolecules 1993, 26, 5535.
17. Pasquet, V.; Spitz, R. Makromol Chem 1993, 194, 451.
18. Calabro, D. C.; Lo, F. Y. In Transition Metal Catalyzed Polymerizations—Ziegler–Natta and Metathesis Polymerizations; Quirk, R. P., Ed.; Cambridge University Press: Cambridge, England, 1988; Chapter 49.
19. Han, T. K.; Ko, Y. S.; Park, J. W.; Woo, S. I. Macromolecules 1996, 29, 7305.
20. Kashiwa, N.; Yoshitake, J. In Transition Metal Catalyzed Polymerizations—Ziegler–Natta and Metathesis Polymerizations; Quirk, R. P., Ed.; Cambridge University Press: Cambridge, England, 1988; Chapter 15.
21. Han-Adebekun, C. G.; Hamba, H.; Ray, W. H. J Polym Sci Part A: Polym Chem 1997, 35, 2063.
22. Atiqullah, M.; Hammawa, H.; Akhtar, M. N.; Khan, J. H.; Hamid, H. J Appl Polym Sci 1998, 70, 137.
23. Sherrington, D. C. Chem Commun 1998, 2275.
24. Zhou, J.-M.; Li, N.-H.; Bu, N.-Y.; Lynch, D. T.; Wanke, S. E. J Appl Polym Sci 2003, 90, 1319.
25. Hammawa, H.; Mannan, T. M.; Lynch, D. T.; Wanke, S. E. J Appl Polym Sci 2004, 92, 3549.
26. Mannan, T. M.; Hammawa, H.; Lynch, D. T.; Wanke, S. E. Can J Chem Eng 2004, 82, 371.
27. Ribeiro, M. R.; Deffieux, A.; Portela, M. F. Ind Eng Chem Res 1997, 36, 1224.
28. Gregg, S. J.; Sing, K. S. W. Adsorption, Surface Area and Porosity, 2nd ed.; Academic: London, 1982; p 154.
29. Broeckhoff, J. P. C.; van Beek, W. P. J Chem Soc Faraday Trans I 1979, 75, 42.
30. Carrado, K. A.; Xu, L. Microporous Mesoporous Mater 1999, 27, 87.
31. Kumkaew, P.; Wanke, S. E.; Praserthdam, P.; Danumah, C.; Kaliaguine, S. J Appl Polym Sci 2003, 87, 1161.
32. Weickert, G.; Meier, G. B.; Pater, J. T. M.; Westerterp, R. K. Chem Eng Sci 1999, 54, 3291.
33. Hamba, M.; Han-Adebekun, G. C.; Ray, W. H. J Polym Sci Part A: Polym Chem 1997, 35, 2075.
34. Grof, Z.; Kosek, J.; Marek, M. AIChE J 2005, 51, 2048.
35. Kittilsen, P.; Svendsen, H. F.; McKenna, T. F. AIChE J 2003, 49, 1495.
36. Chakravarti, S.; Ray, W. H. J Appl Polym Sci 2001, 80, 1096.
37. Camurati, I.; Cavicchi, B.; Dall'Occo, T.; Piemontesi, F. Macromol Chem Phys 2001, 202, 701.
38. Hammawa, H. Ph.D. Thesis, University of Alberta, 2004.
39. Ferrero, M. A.; Koffi, E.; Sommer, R.; Conner, W. C. J Polym Sci Part A: Polym Chem 1992, 30, 2131.
40. Floyd, S.; Heiskanen, T.; Taylor, T. W.; Mann, G. E.; Ray, W. H. J Appl Polym Sci 1987, 33, 1021.
41. Webb, S. W.; Weist, E. L.; Laurence, M. G.; Chiovetta, R. L.; Conner, W. C. Can J Chem Eng 1991, 69, 665.
42. McKenna, T.; Mattioli, V. Macromol Symp 2001, 173, 149.
43. Dalla Lana, I. G.; Szymura, J. A.; Zielinski, P. A. In New Frontiers in Catalysis: Proceedings of the 10th International Congress on Catalysis, Budapest, 1992; Guczi, L.; Solymosi, F.; Tétényi, P, Eds.; Akadémiai Kiadó: Budapest, 1993; p 2329.
44. Bonini, F.; Fraaije, V.; Fink, G. J Polym Sci Part A: Polym Chem 1995, 33, 2393.
45. Hutchinson, R. A.; Chen, C. M.; Ray, W. H. J Appl Polym Sci 1992, 44, 1389.
46. Grof, Z.; Kosek, J.; Marek, M. Ind Eng Chem Res 2005, 44, 2389.